CCFE-PR(15)111

J. C. Flanagan, M. Sertoli, M. Bacharis, G.F. Matthews, P. de Vries,
A. Widdowson , I.H. Coffey , G. Arnoux , B. Sieglin , S. Brezinsek,
J.W. Coenen, S. Marsen, T. Craciunescu, A. Murari, D. Harting,
A. Cackett , E. Hodille and JET EFDA contributors

Characterising Dust in JET with the New ITER-Like Wall

Characterising Dust in JET with the New ITER-Like Wall

J.C. Flanagan[1], M. Sertoli[2], M. Bacharis[3], G.F. Matthews[1], P. de Vries[4], A. Widdowson[1], I.H. Coffey[5], G. Arnoux[1], B. Sieglin[6], S. Brezinsek[7], J.W. Coenen[7], S. Marsen[8], T. Craciunescu[8], A. Murari[9], D. Harting[1], A. Cackett[1], E. Hodille[10] and JET EFDA contributors

[1]CCFE, Culham Science Centre, Abingdon, Oxon, OX14 3DB, UK
[2]Max-Planck-Institut für Plasmaphysik, EURATOM Association, 85748 Garching, Germany
[3]Universite Claude Bernard Lyon I, 69622 Villeurbanne, France
[4]ITER Organization, Route de Vinon-sur-Verdon, CS 90 046, 13067 St. Paul Lez Durance Cedex, France
[5]Queen's University, Belfast, BT7 1NN, UK
[6]Forschungszentrum Juelich GmbH, EURATOM Association, 52425 Juelich, Germany
[7]Max-Planck-Institut für Plasmaphysik, EURATOM Assoc., 7491 Greifswald, Germany
[8]EURATOM-MEdC Assoc., Inst. for Laser, Plasma and Radiation Physics, Romania
[9]Consorzio RFX-Associazione EURATOM ENEA per la Fusione, I-35127 Padova, Italy
[10]Imperial College of Science and Technology, London, UK, SW7 2AZ

ABSTRACT

The results from several studies dedicated to the characterisation of in-vessel dust in JET with the new ITER-like wall (ILW) are reported here. These studies collectively aim to gain insight into the nature of JET's in-vessel dust and its impact on current plasma operations. The techniques used here include the analysis of light scattered from dust mobilized by disruptions and the study of plasma impurities thought to be associated with dust via VUV spectroscopy, together with the analysis of plasma events recorded by JET's camera systems. Some results from a recent in-vessel inspection (which included detailed photo surveys of plasma facing components and dust collection) and results from the numerical modelling of the plasma-dust interaction using the DTOKS and STRAHL codes are also presented.

The key findings from these studies show that the dust levels in the JET ILW are orders of magnitude lower compared with the latter stages of the carbon-wall period, and that dust levels are currently decreasing with operational time. Less than 1g of dust was recovered from the vessel in a recent inspection, compared to more than 200g of material from a similar location at the end of JET's carbon-wall life. Visual inspections show only small areas of mild damage to the vessel interior of a type likely to create particulate matter. Low rates of re-deposition are also inferred from the thin layers (few 100nm) of deposits seen. Quantifiers of the amount of dust in the JET vessel, extracted via laser scattering, also show an order of magnitude reduction from the end of the carbon-wall period. These results also show that the amount of dust mobilized in a disruption is proportional to the dynamic forces on the vessel. It is not possible to infer what fraction of the dust mobilized (if any) might be created by disruptions. However, disruption mitigation via a massive gas injection is found to reduce the amount of dust seen after disruptions of moderate force by a factor of ~ 4.

Analysis of the transient impurity events (TIEs), thought to be associated with dust, show that Tungsten (W) dominates, by half, in all events. A significant contribution to TIEs is also seen from iron, nickel and chromium, most probably originating from the steel and Inconel components in the first wall. The incidence of severe negative effects on plasma operations from TIEs is found to be relatively rare, with < 1% of disruptions from the ILW period to date originating from an impurity event. The evolution over campaign time of the TIE rate closely follows the dust parameters extracted from laser scattering, with both showing an overall downward trend with peaks associated with periods of higher disruption rate. In particular, TIEs are found to be 50% more likely to occur in the four discharges following a disruption. However, since all dust-related measures decrease, on average, with time, the correlation with disruption rate is thought to be primarily driven by the mobilization of existing dust into areas more accessible to the plasma. Results from the DTOKS code, modelling the injection of tungsten dust particles from the outer strike-point at a speed of 10 m/s (as observed by JET camera systems), suggest that a large percentage (~ 40%) of these particles are ablated and deposited in the plasma during TIE events. Simulations using the STRAHL code indicate that the minimum radius of a tungsten particle capable of producing a typical TIE is ~ 50μm.

1. INTRODUCTION

1.1. DUST

In-vessel dust is loosely defined as particulate matter up to ~ 1mm in size and is produced via plasma interaction with plasma-facing components and also via physical trauma during in-vessel maintenance / enhancement works [20]. As such, dust primarily consists of the materials that makeup the in-vessel environment. In JET's current ITER-like wall (ILW) configuration, the plasma facing components (PFCs) principally consist of beryllium (Be) and tungsten (W), with bulk Be tiles and W-coated carbon fibre composite (CFC) tiles and bulk W tiles used in the higher heat flux areas. Nickel, iron and chromium are also present via steel and Inconel components (i.e. supporting structures). Figure 1 shows JET's ITER-like wall, with the different materials shaded according to their composition. For a more detailed description we refer the reader to [18] and references therein.

In-vessel dust has important implications for plasma operations and safety in the tokamak environment, particularly in future long-pulse devices such as ITER [20]. Transient impurity events (TIEs), thought to be caused by small particles or dust contaminating the core plasma, are typified by a sharp increase in radiated power [6 and 23]. TIEs can harm plasma performance and have the potential to lead to instability events and can abruptly terminate the plasma discharge [11, 13 and 23]. Large volumes of dust also present safety issues in terms of tritium retention and the potential for volatile interaction in the event of air or water ingress into a hot vessel. [4 and 21]. The current ITER strategy in response to these concerns is to measure and minimise the dust inventory [20]. Building an understanding of dust characteristics and their impact on plasma operations within current devices is thus essential to this goal.

1.2. DISRUPTIONS

During a disruption, the growth of plasma instabilities impairs confinement and causes a rapid and large loss of thermal energy (referred to as the thermal quench). This typically leads to the loss of plasma current (the current quench) and is often accompanied by a loss of vertical stability, called a vertical displacement event [11]. The fast release of magnetic energy often results in large forces transferred to the mechanical structure of the vessel, causing it to shake. Disruption forces of up to 4MN have been recorded at JET (in both CW and ILW operational periods), with disruption forces of > 1MN commonplace. During the thermal quench, high heat-loads can also be transferred onto the PFCs. The relatively delicate nature of JET's ILW (Be melts at ~ 1300°C) has necessitated the development of disruption mitigation methods based on a massive gas injection (MGI), delivered just prior to plasma termination [17]. Mitigation by MGI has been shown to significantly decrease the sideways forces during vertical displacement events. The heat loads during the thermal quench can also be reduced by the enhancement in energy radiated from the plasma that is seen with MGI [11 and 17]. Timing parameters relating to JET disruptions are defined here as: the disruption time t_d, which is equal to the onset of the thermal quench; and the time of maximum vessel displacement t_m, which marks the point at which one may expect to see disruption related mobilization occurring.

1.3. OVERVIEW

In this work, we aim to provide answers to some key questions on the topic of in-vessel dust for JET's new ILW; *e.g.* how much dust is there and what is it made from? How does this compare to previous phases of operations with the CFC wall? What are the sources of dust and what impact does the current dust inventory have on plasma operations? Are there particular events that we should strive to avoid in terms of dust production / mobilization? How is the amount of dust changing with time? At what point does the dust inventory become a real problem and is active mitigation necessary? What does this mean for future devices, such as ITER? Answering these questions is only possible by studying the properties of the in-vessel dust at frequent intervals, including dust related events occurring during plasma operations. Consequently, remote methods of dust and TIE analysis are essential and are considered in addition to the assessment of information and material gathered during in-vessel studies (for which manned access is, briefly, necessary). Theoretical modelling of the interaction of plasma and dust is another valuable source of information; one that has the potential to bridge the gaps in knowledge obtained through remote observations and can also give a deeper understanding of the physical mechanisms responsible for impurity radiation events. The methods considered here are:

1. Images of events during operations from JET's numerous camera-based monitoring systems
2. VUV spectroscopy of TIEs during plasma discharges
3. Analysis of photo surveys and dust collection performed during a recent in-vessel inspection
4. Laser scattering from dust mobilized by disruptions
5. Numerical modelling of the plasma dust interaction

The experimental methods of observing dust and related events are described in detail in Section 3, together with results for JET's recent operational period with the ILW. Where possible, comparisons to results from JET's carbon-wall (CW) period are made. Results from numerical modelling work on the dust plasma interaction are reported in Section 4. Discussion and conclusions are presented in Section 4.

2. EXPERIMENTAL METHODS AND RESULTS

A summary of results from four methods of monitoring in-vessel dust are presented here; a) camera imaging, b) VUV spectroscopy, c) in-vessel inspection (including physical dust collection) and d) laser scattering after disruptions.

2.1. CAMERA SYSTEMS

JET houses numerous visible and infrared camera systems used to make real-time observations of the plasma chamber; to monitor the plasma itself, as well as the plasma facing components. A systematic analysis of this type of data over the many thousands of JET pulses is a formidable task, and not one that we consider here. Instead, we look to this source of information for a few

events of particular interest; to assist in the understanding and the benchmarking of data from other sources and to highlight events for further study. However, we note that the automatic analysis of defects (such as particulate matter) on the horizontal surfaces of JET's divertor tiles has been demonstrated [9].

JET's camera systems are often particularly illuminating in the case of disruptions and often capture particles shaken loose by the vessel displacement, as seen in Figure 2 and Figure 3, which show sequential video frames from the KL1 camera for JET pulse 80706 and 80652 respectively. In both instances a cloud of glowing debris is visible just after the disruption. The dust in Figure 2 appears to be rotating, centred around the middle of the vessel, while the dust in Figure 3 moves from the vessel centre to the outer divertor region and does not rise above the mid-plane of the vessel. The fact that dust does not uniformly fill the vessel in these events is important when interpreting data from diagnostic systems with narrow lines of sight.

Disruptions can also lead to high heat-loads onto the PFC, which are closely monitored by JET's infrared protection camera systems [1]. In extreme heat-load events, melting of parts of the Beryllium PFCs as the plasma terminates has been observed. In JET pulse 85943, an experiment studying runaway electrons disrupted after the runaways doubled past the intended number. The resultant high heat-load on the upper dump plates caused partial melting. Droplets of beryllium were seen to rain down into the divertor region, as shown by the video frames from KL14, a high resolution DSLR camera, in Figure 4. This is JET's most sensitive visible camera; the slight distortion in the image is due to the complex optics of this system, which includes in-vessel mirrors [5].

The influx of particles into the JET plasma is also sometimes captured by camera systems; see examples in Figure 5. JET pulse 80406 disrupted soon after the particle influx shown in Figure 5 (a) – (c), while the particles seen entering the plasma in JET pulse 84645 (Figure 5 (e)) resulted in a large TIE and significantly lowered the pedestal temperature. In both of these cases, VUV analysis identified tungsten as the responsible impurity (see Section 2.3 for more details). Images of this type allow the particle trajectory and velocity at input to be approximated; parameters which will serve as useful inputs to any modelling effort (see Section 4).

2.2. VUV SPECTROSCOPY OF IMPURITY EVENTS

Transient impurity events (TIEs) are also known as UFOs as they often appear as bright flying objects and are thought to result from small particles or dust contaminating the core plasma. TIEs are characterised by large, often short-lived, spikes in radiated power [6 and 23]. An example of these impurity driven radiation events is shown in Figure 6 (a) – (c). Please refer to the figure caption for more details. These radiation events have a typical rise time of ms and can, in some cases, lead to a long-lasting growth in radiated power. In severe cases, this can add up to ~ 1 MW to the steady-state bulk radiated power – a significant contribution. In the most extreme cases, these radiation events can lead to plasma instabilities and even termination of the plasma discharge (an example of the latter is pulse 80406 from Figure 5) [11, 13 and 23].

Data from two of JETs VUV survey SPRED spectrometers have been used to investigate the elemental composition of the impurities related to TIEs [23]. These systems monitor the impurity content of the JET plasma across the spectral ranges 100 – 1000 Å and 140 – 443 Å, along lines-of-sight at octant 6 (shown in the poloidal cross-section in Figure 6(a)) [8, 14 and 25]. By integrating the VUV signal over known spectral emission lines, events originating from Ni, Fe, Cr, Cu, Al and W impurities can be distinguished. Example data for three sequential TIEs in the same pulse resulting from W impurities is shown in Figure 6 (c).

The occurrence of TIEs has been analysed for JET pulse 80128 to 85699, which starts with the very first campaign of JET's new ILW [23]. A total of 3388 events have been detected in 4144 plasma discharges (~ 23 hours of plasma), with an average of 1 event every 25 seconds of plasma.

This study shows that the major contributor to TIEs is W, accounting for 51% of all impurity events, with W usually occurring in isolation. 26% of all events are correlated with the simultaneous presence of Ni, Fe and Cr, which almost certainly originate from Inconel or steel in-vessel components. The remaining percentage of events corresponds to either Al or Cu, or to events with no clear VUV signature in the spectral range considered (these may result from lighter elements, such as carbon and beryllium). Over the initial ILW operation period, 22 impurity events are induced by material flaking from the reciprocating probe (RCP) diagnostic, used to measure the electron temperature at the upper edge of the JET plasma at octant 5 [10]. These events are dominated by Ni, Fe and Cr, which is consistent with the material of the probe shaft (Inconel / steel).

A database containing various parameters for every plasma discharge in the TIE analysis pulse range has also been collated in order to explore parametric dependencies [23]. A clear correlation with disruption events is found; TIEs are most likely to occur in the few discharges following a disruption, with the TIE rate 50% higher in the 4 discharges following a disruption. Figure 7 shows the TIE and disruption rate (defined as the number of events per bin, normalised to the total plasma operational time for the discharges in that bin), with a bin width of 300 JET pulses. A strong correlation between the TIE and disruption rate is apparent, with three discreet peaks seen in each data set. The peaks in disruption rate correspond to intentional disruptions associated with experimental sessions studying disruptions, disruption mitigation techniques and runaway electron events. The majority of disruption events in these periods are intentionally induced with typically high displacement forces. The TIE rate follows a very similar trend, with an additional overall downward drift; one that is particularly noticeable for JET pulse < 81200, where the TIE rate decreases by a factor of three in spite of the rise that occurs in the disruption rate over this time. This initial drop is also mirrored in the HRTS dust signal (see Section 4.3 for more details). Taken together, these results suggest that an initial inventory of dust, present from the very start of ILW operations, is being gradually removed from circulation. The rises associated with periods of frequent disruptions may indicate that disruptions redistribute dust into more accessible areas. It is not possible to infer from this if disruptions create new dust material.

The study in [23] has also shown that TIEs are far more likely in diverted plasma configurations

with the probability of a TIE occurring significantly reduced if the strike point is located on the vertical surface of a divertor tile, as opposed to a horizontal surface. This seems logical, given that dust tends to collect on the horizontal surfaces of the divertor region. Overall, the probability of a severe outcome from a TIE is low; only 25 of the 3388 TIEs studied result in a significant (> 60%) drop in plasma energy. And of these, less than 10 result in a disruption in the few seconds after the TIE (c.f. with ~ 700 disruptions over the ILW period).

2.3. IN-VESSEL INSPECTION

There are many erosion-deposition diagnostic tools installed into JET's ILW, including beryllium and tungsten marker tiles and wall probes in the main chamber and divertor [22]. During a recent intervention period (just after JET pulse 83934) with in-vessel access, these diagnostic tools have been recovered for analysis with detailed in-vessel photographic surveys and dust collection also performed [24]. Here, we present a brief summary of some of the initial dust related findings from these studies. The post-mortem analysis from these studies will continue for some time.

A selection of images from the detailed photographic survey are shown in Figure 8 (a) – (c) together with an infrared image from the KL7 camera in (d) showing the heat loads on the JET ILW during a density limit disruption pulse (JET pulse 81550). This is shown to illustrate some of the areas of JETs PFCs most at risk. The image in (a) shows damage due to melting and arcing on one of the bulk Be upper dump plate tiles. The images in Figure 8 (b) and (c) correspond to the upper horizontal surface of the divertor tile 8. In (b) delamination of the W coating is seen, with small bead of W visible at the ends of some of the damaged strips. These regions of delamination lie along the CFC fibres and are not seen on all tiles: some are noticeably worse than others. This probably results from the fact that the CFC proved difficult to coat with W [18]. In (c), a small droplet of Be can be seen, possibly originating from the upper dump plate above.

Dust collection from the divertor region yielded ~ 1g of material – significantly less than the 200g recovered from the same area during the CW period [24]. Compositional analysis on the dust extracted from the divertor is in progress. Studies of deposition diagnostics reveal that the quantity of deposits in the divertor region is an order of magnitude less than for the CW, with deposits of only a few 100nm thick observed so far [24]. This reduction in migrated material may be linked to the drop in dust collected to date since there will be a significantly increased time for layers to reach mechanical stability limits. The overall picture from this analysis is that the ILW is a much cleaner environment than the CW, but that mechanisms do exist for the production of W and Be particulates.

From inspection of the TIE data, we see that there are approx. 1700 events that can be attributed to W across the operation of the ILW. If we assume that the W concentration spikes to approximately 10^{-4} (an upper estimate) in each instance, and assume a volume average electron density of order $10^{20}m^{-3}$, we can estimate that there are somewhere in the region of 10^{18}W atoms per TIE (JET plasma volume ~ $100m^3$). A maximum estimate of the W particle mass required for all observed W TIEs is then ~ 0.3g. The 1g of dust recovered from a portion of divertor

thus demonstrates that there is almost certainly sufficient material (assuming the dust has a representative proportion of W as seen in the TIEs). However, many parameters influence how impurity particles interact with the plasma (i.e. particle size, injection velocity, plasma parameters) and screening may prevent them from entering the core at all. A deeper understanding of this interaction can only be answered with a far more sophisticated analysis; such as the numerical modelling described in Section 4.

2.4. LASER SCATTERING

JETs high resolution Thomson scattering (HRTS) diagnostic is a conventional Thomson scattering system [19], which has been routinely producing electron density and temperature profiles of the JET plasma since 2007. This system uses a 5 J pulsed Nd:YAG laser fired into the JET vessel through a vacuum window located roughly mid-plane at octant 5 (see Figure 6(d)). The HRTS diagnostic provides 35 seconds of data from the start of a JET discharge with a spatial resolution of approx. 1.5cm. During a plasma discharge, Thomson scattered light from the laser chord is analysed by a bank of spectrometers. In the few seconds immediately following a disruption, large spikes are often seen in the HRTS signal, as shown in Figure 9 (a). These signal spikes originate from the interaction between the laser beam and dust mobilized by the disruption [15]. The long decay time of the dust signal detected by the HRTS spectrometers, shown in Figure 9 (b), is typical of light emitted from a source that has been heated or ablated by a laser pulse. Typically, dust signals are detected for a period of approx. 1-3 seconds following a disruption.

The HRTS system thus provides an automatic measure of the quantity of dust mobilized by a disruption event. However, the limitations of this technique should be appreciated; the volume of the JET vessel sampled by the HRTS laser chord is very small and signal is only detected if dust passes through this particular region of space at octant 5. There are cases noted where dust / debris is visible on JETs camera systems in regions that do not intersect the HRTS chord. An example of this was shown previously in Figure 3. In this instance, the cloud of particles stays below the HRTS line-of- sight and no HRTS dust signal is detected. In addition, it is not simple to infer particle size from the event magnitude, since different materials are expected to have different intrinsic brightness when interacting with the pulsed laser. Surface quality and any surface coatings present may also play a role in determining the brightness of any given dust-laser interaction event. Furthermore, it is not possible to distinguish between many particles in close proximity and a single large event, and a particle moving along the laser chord will be recorded as multiple events. When added to the fact that this measure of the dust inventory is only made infrequently (i.e. with disruptions), one must be cautious about interpreting the resulting data. However, by analysing the HRTS signal across many disruption events, we find that it is possible to extract trends and explore relationships.

The parameters that are extracted from the HRTS dust signal for analysis are:

1. The total signal (T_{sig}): this is the integrated signal level of all dust events detected in a single disruption; i.e. the total ‘brightness’.

2. The total number of events (N_{dust}): this is the total number of signal spikes detected in a single disruption; i.e. the number of dust particles (to first order approximation).

These parameters can be generated automatically using a variant of the code used to provide the electron temperature and density data from this diagnostic. HRTS dust data is available for 363 disruptions in the very latter part of the CW period (for JET pulse 73337 to 79853) and for 695 disruptions in the period of operation to date with the ILW (for JET pulse 80128 to 85978). The most striking result from this analysis is that the amount of dust seen is significantly smaller for the ILW than for the CW period, by a factor of 20 (on average) for the total dust signal and a factor of 30 (on average) for the number of dust events. This is in rough agreement with the differences in the mass of dust collected from the vessel during CW and ILW intervention periods (see Section 3.3 for more detail).

Further analysis shows that there is a clear positive correlation between the disruption force and the HRTS dust parameters, as shown in Figure 10 (a) which shows T_{sig} for both the CW (blue) and ILW (red) as a function of disruption force. Please see the figure caption for further details. A very similar relationship is seen for N_{dust} (not shown here for brevity). This relationship confirms a somewhat intuitive expectation; that the amount of dust shaken free is proportional to the vessel displacement forces. However, as for the case of the TIE analysis, this provides no information on what fraction of dust might be created by a disruption as opposed to merely mobilized.

Information on the effect of disruption mitigation via massive gas injection (MGI), known to reduce forces and heat loads, can also be gained from the HRTS dust data. In Figure 10 (b), the ILW T_{sig} data from (a) is re-plotted, with all events split into two data sets: accounting for whether or not MGI was used to mitigate the disruptions. Both data sets show the same increasing trend with disruption force, with a difference in magnitude. The amount of data here is somewhat limited, with error bars producing overlapping data sets for much of the force range. However, for the second force bin, located at ~ 1.25MN, it can be seen that there is a clear drop with the average T_{sig} reduced by a factor of 1.6 (on average) in the case of MGI (N_{dust} is similarly reduced, by a factor of 1.9). Note that this observed reduction in dust is for disruptions of the *same* force. When the force reduction of the MGI is taken into account, this demonstrates that the use of MGI can reduce the mobilized by a disruption by approximately a factor of 4.

The evolution of the HRTS dust signals over the first five campaigns of the ILW period (covering JET pulse 80128 to 85977) is shown in Figure 11. Light blue and red points with vertical markers show data for individual disruptions. Dark blue and red points show average values for a bin width of 300 pulses. The individual disruptions with values far higher than the global average are explained in Figure 12(a) and surrounding text. In the initial period (up to JET pulse 81400), there is a rapid decline, with the drop in N_{dust} closely mirroring the fall in the rate of TIE seen over this period. As previously mentioned, this suggests that material present prior to the start of the ILW plasma operations has been gradually removed from circulation. Small particles of debris visible on

images of divertor tiles taken before ILW operations began, shown in Figure 11 (d), add weight to this theory. Images of the same tiles taken just after JET pulse 82929 when both the TIE and HRTS signal levels are significantly reduced are clear of debris. Inset, in Figure 12(b), the evolution of T_{sig} past the initial period of steep decline is shown (for JET pulse > 81400). Here, several peaks in T_{sig} can be seen, superimposed on an overall downward trend, which match the fluctuations in the TIE rate over the same period (plotted in blue). This correlation adds further weight to the theory that TIEs are caused by dust particles.

While T_{sig} and N_{dust} show a strong correlation (on average) and both display similar trends with disruption force, their ratio shows a large degree of variation. In an attempt to further understand this, we find it useful to plot T_{sig} as a function of N_{dust} for each disruption, as shown in Figure 12 (a).

Displaying the data in this way allows the most extreme events to be clearly identified. By exploring the details of these events, we see patterns emerge; the events in Figure 12 with high values of both T_{sig} and N_{dust} (circled) correspond to discharges in which the reciprocating probe (RCP) diagnostic was malfunctioning, introducing material into the vessel. As mentioned in Section 2.3, VUV analysis has shown that impurities associated with these events are consistent with the materials of the probe shaft [23].

The disruptions with very high values of T_{sig} but lower values of N_{dust}, are all found to lie in the very early part of the ILW operational period – within the first 10 disruptions. On closer inspection of the HRTS data we see that, in each case, the very high signal level can often be attributed in the major part to just a few dust events. This suggests that the high values of T_{sig} after disruptions at this time period may have resulted from a few large dust particles that were later fragmented / eroded. Other high magnitude events are also found to be associated with an influx of material, within that same pulse, from a range of sources. These are indicated in the legend on Figure 12 (a) and include tungsten influx from the divertor region (as shown in Figure 5), beryllium droplets from melt damage (as described in Figure 4 and Figure 8 (a) and surrounding text), in addition to copper influx (possibly from the neutral beam injection system).

3. NUMERICAL MODELLING

Modelling of the transport and ablation of tungsten dust particles in the JET plasma has been carried out using the 2-D code DTOKS [3]. This model assumes spherical dust particles and includes the effects of heating and electrostatic charging, in addition to the effects of the Lorentz force, ion drag and gravity. The inputs to the model are the dust particle size, composition and the initial injection position, angle and velocity, in addition to plasma parameters. Here we show the result from a subset of this work, which considers W particles, injected from the outer strike point with an initial velocity of 10 m/s since this correlates well with observed behaviour, shown in Figure 5. The DTOKS code is used to look at the effect of particle size for a full range of injection angles (–70° to +70° relative to surface normal). Particle sizes of 100, 75, 50, 25 and 10 μm are considered with plasma parameters from JET pulse 82550 at t = 15.5.

The results from this case, shown in Figure 13, predict that the fraction of a particle's mass ablated inside the plasma increases with particle size for particles < 20μm, with a subsequent plateau at a value of ~ 40%. In related works, the 1-D STRAHL code has also been used to simulate the impurity transport occurring after the dust ablation from this DTOKS study [12 and 23]. Estimates from this approach indicate that the number of ablated ions needed to generate the observed increase in radiated power is of the order of 2×10^{17}. Accounting for the fraction of material ablated, this suggests that a minimum W particle size of ~ 50μm is required in order to obtain a radiative event similar to the typical TIE observed in JET plasma discharges with the ILW.

Accounting for the total number of W-TIEs (1697), this estimates that ~ 0.2g of W dust is required; in good agreement with the previous crude estimates from Section 3.3. Note also that this estimate of particle size is similar to the size of the droplets seen during the bulk-W melt experiments [7].

4. DISCUSSION AND CONCLUSIONS

The results presented here have shown that the amount of dust for the ILW is low and, at present, is decreasing with operational time. These results also suggest that disruptions primarily act to mobilize the existing quota of dust, moving a subset of this material into areas more accessible to the plasma. These re-positioned dust particles are then more likely to appear as transient impurity events (TIEs) in subsequent plasma discharges, where they are partially consumed and later re-deposited as thin films onto the plasma facing components. It should be noted that the methods used here are very poor indicators of how much of the dust seen after a disruption might be created in that event, as opposed to merely mobilized. The fact that dust levels are decreasing with time despite relative frequent disruptions (many of them deliberately induced for studies of disruption physics etc.) suggests that little, if any, dust is created during a disruption. However, for moderate disruption forces, the amount of dust seen for mitigated disruptions is notably reduced. Since mitigated disruptions lower heat loads to the plasma facing components, this may indicate that unmitigated disruptions do indeed create some material.

The high TIE rate and (relatively) large amounts of dust seen after disruptions during the early period of operation with the ILW points to material left in the vessel after the installation of the ILW was completed. Over time, these particles appear to have been gradually removed from circulation (via processes of erosion / fragmentation and possible re-positioning into in-accessible areas, such as the spaces behind the first wall tiles). Some events during plasma operations have also been seen to add to the quota of particulate matter, but, at present, the rate at which this material is removed from circulation is greater than any accumulation. As re-deposited layers build up and reach mechanical stability limits, this may change. However, the rates of material migration are orders of magnitude lower than for the carbon-wall and this may not happen for some time.

The effect of dust particles on plasma operations seems to be tolerable, with large losses to plasma energy or confinement relative rare. However, a few (of the handful) of impurity induced disruptions account for some of the most extreme disruptions in the ILW history to date; the highest

disruption forces for an unintentional disruption, of 3.21MN, occurred after a large W-influx from the divertor region. However, it should be noted that in this case, the disruption was unmitigated. The, now more routine, use of a massive gas injection in response to disruption precursors will obviously lessen the impact of such events.

The numerical modelling of the transport and ablation of W dust particles in the JET plasma confirm that W particles of a feasible size are capable of generating radiation events of the magnitude seen in JET plasmas. This modelling work also helps to confirm that there is sufficient material generated from the (relatively small amounts) of damage seen to the tungsten parts of the plasma facing components to account for the number of TIEs seen during the operation period of the ILW to date. Further studies of particle influx in images from JET camera systems and analysis of the collected dust in terms of size and composition should allow for further refinement of input parameters to these models.

In conclusion, although impurities from in-vessel dust can, in extreme cases, have undesirable effects on plasma performance, taken together, the results shown here are encouraging for future devices such as ITER. The recent operational period of JET with the ILW has demonstrated that despite an initial inventory of material, and with repeated additions to this inventory, there exist efficient mechanisms that act to remove dust from circulation during normal plasma operations. Furthermore, since dust particle sizes are unlikely to scale with the vessel dimensions, the relative impact of individual impurities events should reduce for larger devices, such as ITER.

ACKNOWLEDGEMENTS

This work was supported by EURATOM and carried out within the framework of the European Fusion Development Agreement and the RCUK Energy Programme [grant number EP/I501045]. The views and opinions expressed herein do not necessarily reflect those of the European Commission or ITER.

REFERENCES

[1]. Arnoux, G., 2010. Heat Load Measurements on the JET First Wall during Disruptions. San Diego, California, USA, Proceedings of the 19th International Conference on Plasma Surface Interactions.

[2]. Arnoux, G., 2014. Power handling of the JET ITER-like wall. Physica Scripta, **2014**(T159), p. 014009.

[3]. Bacharis, M., 2010. Dust in tokamaks: An overview of the physical model of the dust in tokamaks code. Physics of Plasmas (1994-present), **17**(4), p. 042505.

[4]. Bell, A., 2002. Tritium Inventory Control – the Experience with DT Tokamaks and its Relevance for Future Machines. Helsinki, Finland, Proceedings of SOFT 2002.

[5]. Clever, M., 2013. A wide angle view imaging diagnostic with all reflective, in-vessel optics at JET. Fusion Engineering and Design, Volume **88**, pp. 1342–1346.

[6]. Coenen, J., 2013. Long-term evolution of the impurity composition and impurity events with the ITER-like wall at JET. Nuclear Fusion, **53**(7), p. 073043.

[7]. Coenen, J., 2014. ELM induced tungsten melting and its impact on tokamak operation. Kanazawa, Japan, Proceeding of the 21st International Conference on Plasma Surface Interactions (PSI).

[8]. Coffey, I., 2004. First tritium operation of ITER-prototype VUV spectroscopy on JET. Review of Scientific Instruments, Volume **75**, p. 3737.

[9]. Crasciunesco, T., 2014. Overview of Image Processing Tools to Extract Physical Information from JET Videos. Proceedings of the 8th Workshop on Fusion Data Processing, Validation and Analysis, pp. 4th November – 6th November 2013.

[10]. Davies, S., 1996. The JET Reciprocating Probe Systems – Performance and Data Analysis. Contributions to Plasma Physics, **36**(S1), pp. 117–123.

[11]. de Vries, P. C., 2014. The influence of an ITER-like wall on disruptions at JET. Physics of Plasmas (1994–present), **21**(5).

[12]. Dux, R., 2006. STRAHL User Manual, IPP Garching: Laborberiicht 10/30.

[13]. Ekedahl, A., 2009. Analysis of radiative disruptions in RF-heated Tore Supra plasmas using infrared imaging. Journal of Nuclear Materials, **390–391**(15 June 209), pp. 806–809.

[14]. Fonck, R., 1982. Multichannel grazing incidence spectrometer for plasma impurity diagnosis: SPRED. Applied Optics, **21**(12), p. 2115.

[15]. Giovannozzi, E., 2010. Detection of dust on JET with the high resolution Thomson scattering system. Rev. Sci. Instrum., **81**(10), p. 10E131.

[16]. Huber, A., 2012. Development of a mirror-based endoscope for divertor spectroscopy on JET with the. Review of Scientific Instruments, p. 10D511.

[17]. Lehnen, M., 2010. Disruption Mitigation by Massive Gas Injection in JET. Daejon, Republic of Korea, Proceedings of the 23rd IAEA Fusion Energy Conference.

[18]. Matthews, G. F., 2011. JET ITER-like wall—overview and experimental programme. Physica Scripta, 2011(**T145**), p. 014001.

[19]. Pasqualotto, R., 2004. High resolution Thomson scattering for Joint European Torus (JET). Review of Scientific Instruments, **75**(10), p. 3891.

[20]. Rosanvallon, S., 2009. Dust limit management strategy in tokamaks. Journal of Nuclear Materials, **390–391**(15 June 2009), pp. 57–60.

[21]. Roth, J., 2009. Recent analysis of key plasma wall interactions issues for ITER. Journal of Nuclear Materials, 390–391(15 June 2009), pp. 1–9.

[22]. Rubel, M., 2013. Overview of erosion-deposition diagnostic tools for the ITER-Like Wall in the JET tokamak. Journal of Nuclear Materials, **438**(01), pp. S1204-S1207.

[23]. Sertoli, M., 2014. Impact of W events and dust on JET-ILW operation. Ongaku-do, Kanazawa Ishikawa, Japan, s.n.

[24]. Widdowson, A., 2014. Material Migration Patterns and Overview of First Surface Analysis of the JET ITER-like Wall. Julich, Germany, Proceedings of the 14th International Conference of Plasma-Facing Materials and Components for Fusion Applications.

[25]. Wolf, R., 1995. A vacuum Ultra-violet Spectrometer (Double_SPRED) for the Observations of the JET Divertor Plasma. Submitted to Review of Scientific Instruments.

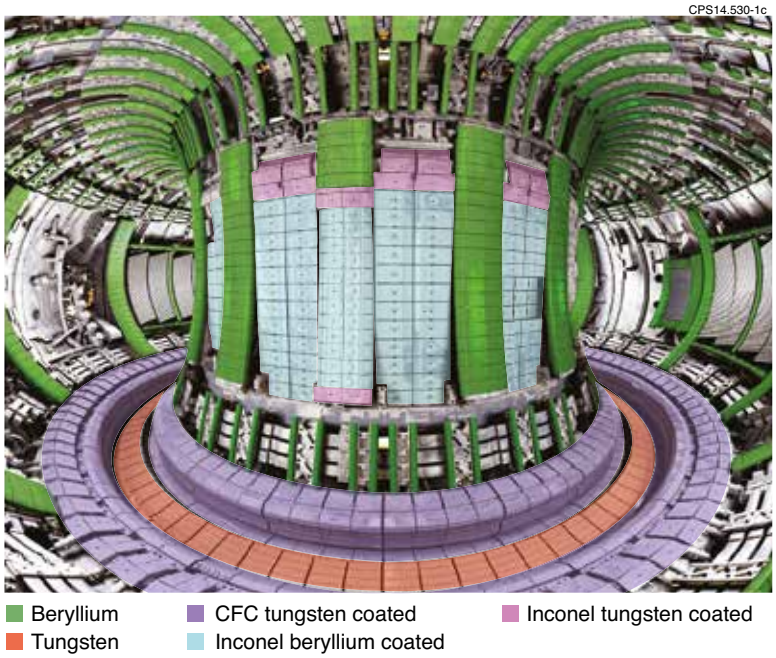

Figure 1: Photograph of the JET ITER-Like Wall (ILW). Coloured shading indicates material composition.

Figure 2: Frames from Images from JET's COHU colour CCD camera (KL1) from octant 4 for JET Pulse No: 80706. The plasma is terminated by a disruption with t_d = 14.168s and t_m = 14.25s. Induced vessel forces are recorded as 2.52 MN. A cloud of debris is seen at t = 14.24s and in subsequent frames.

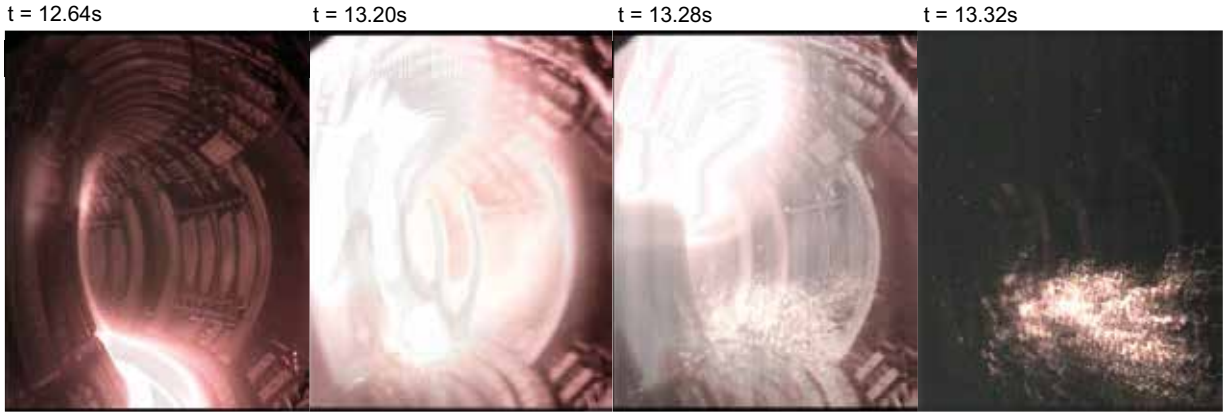

Figure 3: Images from JET's COHU colour CCD camera (KL1) from octant 4 for JET Pulse No: 80652. The plasma is terminated by a disruption with t_d = 13.14s and t_m = 13.18s. Induced vessel forces are recorded as 0.43MN. A cloud of debris is seen at t = 13.20s and in subsequent frames. Note that the images in frames after t = t_d show distortion due to camera shaking.

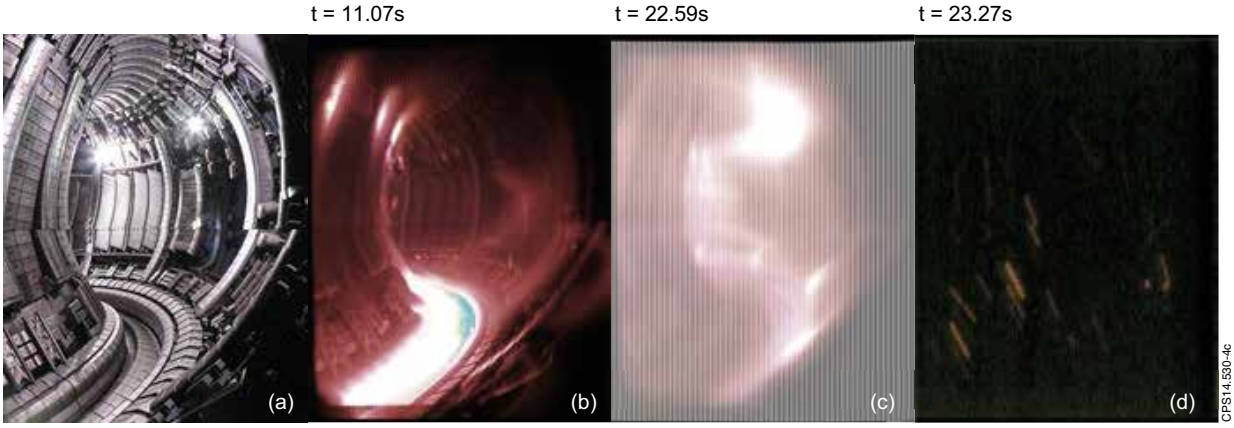

Figure 4 (a) View from octant 5, as seen by the high resolution DSLR camera (KL14) with the internal vessel lights on. (b) – (d) Frames from KL14 for JET Pulse No: 85943. The plasma is terminated by a disruption with t_d = 22.53s and t_m = 22.59s. Induced vessel forces are recorded as 0.90MN. (d) Sometime after the initial disruption (at t = 23.10s onwards), particles can be seen falling from an upper part of the vessel into the divertor region.

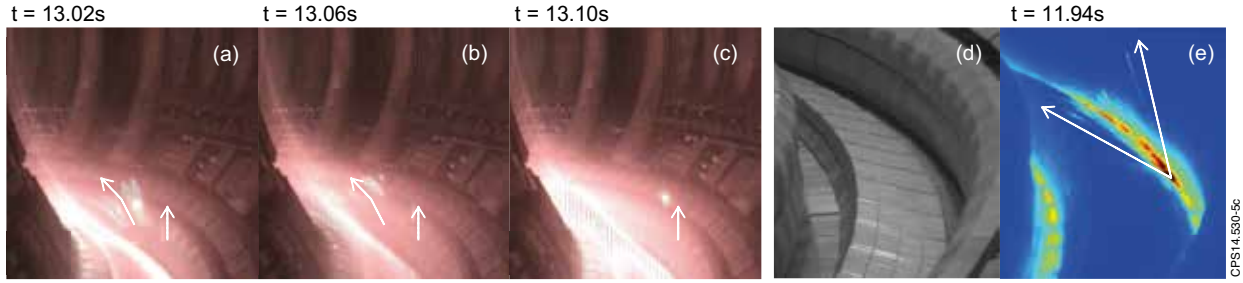

Figure 5 Images showing influx of particulate matter into the JET plasma. (a) – (c) JET's COHU colour CCD camera (KL1) from octant 4 for JET Pulse No: 80406, (d) Divertor view from octant 1 as seen by the AVT-PIKE camera (KL11) [16], with the internal vessel lights on (e) frame from KL11 for JET Pulse No: 84865.

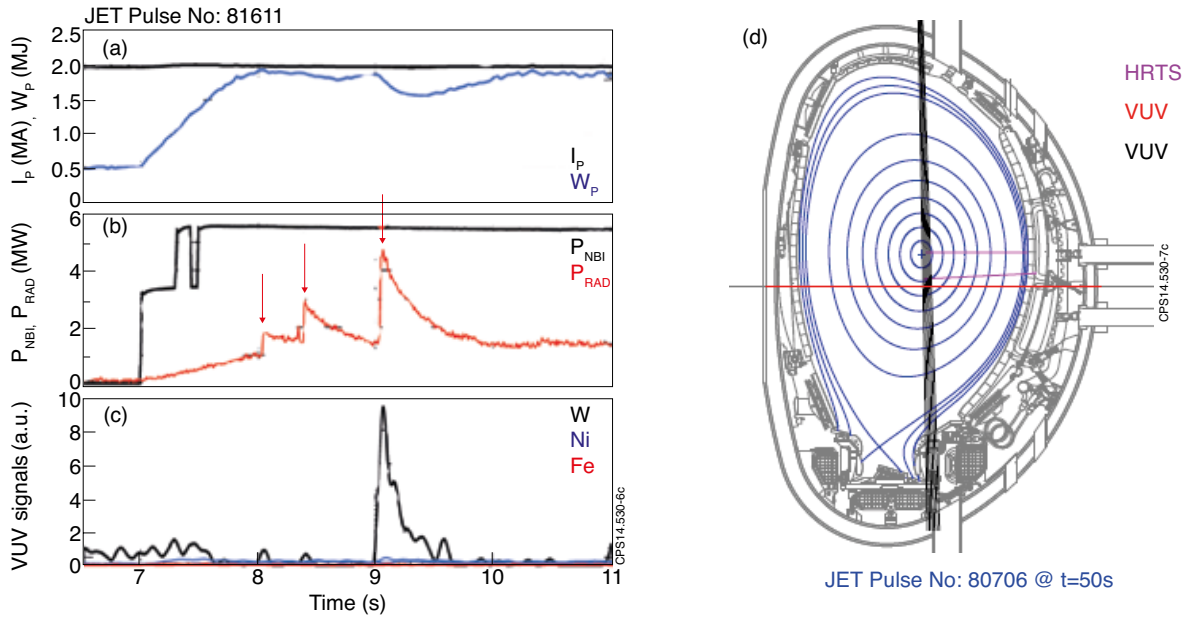

Figure 6 (a) – (c) Example of TIE occurring in JET Pulse No: 81611 from [23] (a) plasma current and energy, (b) NBI and radiated power, (c) VUV data for W, Ni and Fe lines. (d) A cross-sectional view of JET, showing the diagnostic lines-of-sight for HRTS (octant 5), two VUV diagnostics (both octant 6). Magnetic flux lines for JET Pulse No: 80706 at t = 50 s are shown for illustrative purposes.

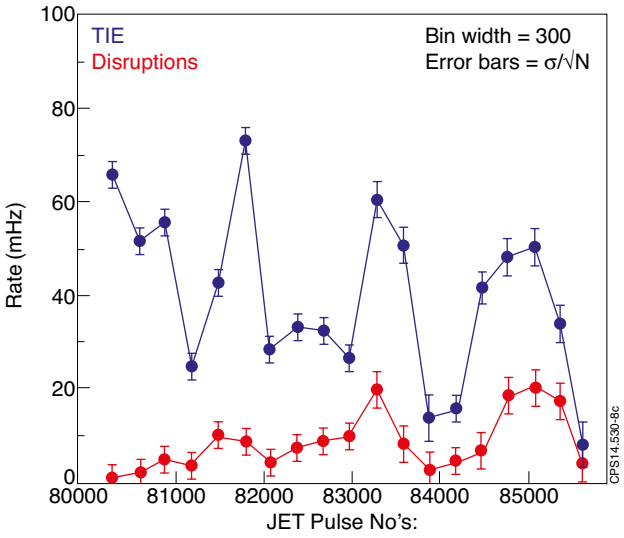

Figure 7 The TIE and disruption rate (normalised to plasma operational time) as a function of JET pulse number (JPN)

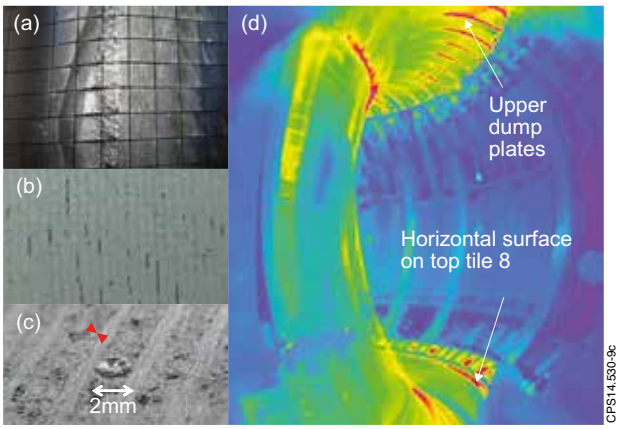

Figure 8 (a) Upper dump plate (bulk-Be) showing melting in the centre and the results of arcing on the right hand side [2]. (b) and (c) Show images from the horizontal surface on top tile 8 (W-coated CFC). In (b), delamination of the W-coating with small beads of W are visible. (c) Shows a small Be droplet. (d) Infrared image from the KL7 camera showing the heat loads on the JET ILW during a density limit disruption pulse; JET Pulse No: 81550.

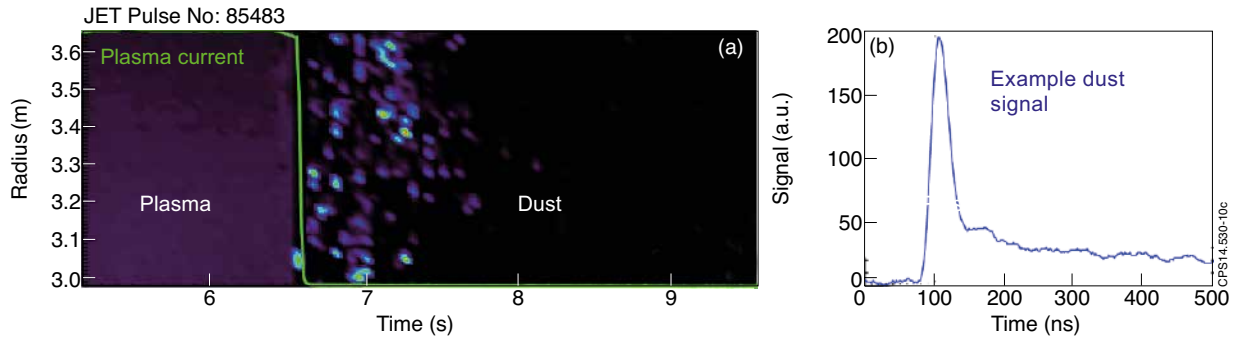

Figure 9 HRTS (a) Colour levels show the HRTS signal for JET Pulse No: 85483 as a function of time. The plasma is terminated by a disruption with t_d = 6.56s and t_m = 6.65s. Induced vessel forces are recorded as 0.75MN. At the time of the disruption, the plasma current (superimposed schematically in green) plummets to zero. At this time, the HRTS signal changes from Thomson scattered light, visible on all spectrometers, to an intermittent dust signal with a characteristic temporal signature, shown in the example in (b).

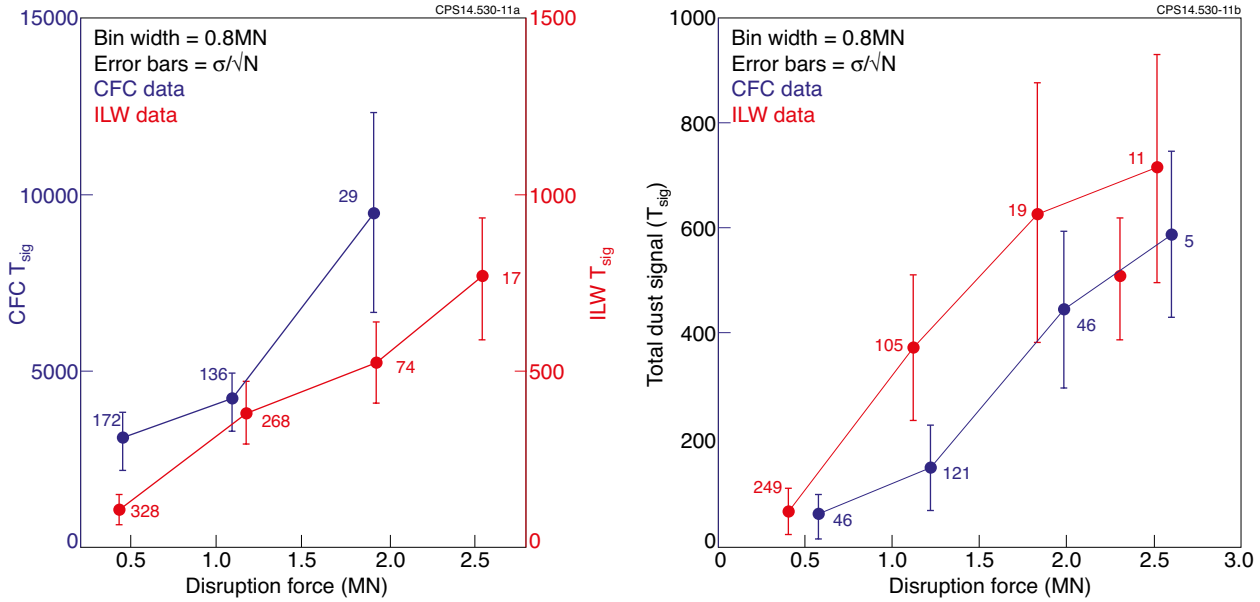

Figure 10 (a) HRTS total dust signal T_{sig} for both the CW (blue) and ILW (red) as a function of disruption force. Note that the CW data is plotted on a vertical scale 10 times larger than for the ILW data. Each data point corresponds to the average value in a bin of width 0.8MN with error bars of to σ/√N, where N is the number of disruption events in that bin and σ is their standard deviation. The value of N is shown on the figure, next to the corresponding data point. (b) A similar plot as (a), but for ILW data only, for disruptions with (blue) and without (red) use of disruption mitigation via massive gas injection. Data in (b) only includes pulses for which the disruption mitigation system was fully active: JET Pulse No's: 81560 – 85977.

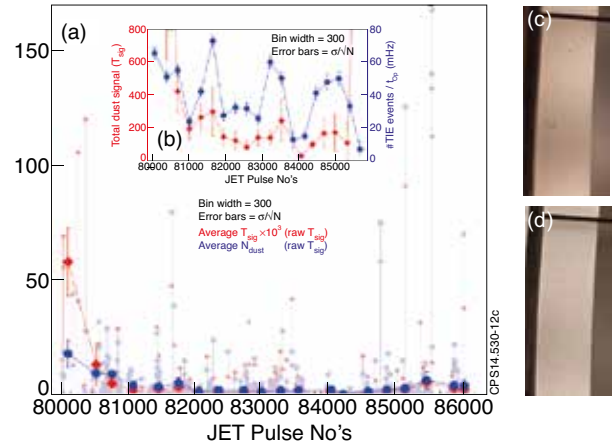

Figure 11 : (a) HRTS T_{sig} (diamonds) and N_{dust} (circles) as a function of JET Pulse No's: 80128 – 85977, corresponding to the first 5 campaigns of the ILW period. Light blue and red points with vertical markers show raw data for individual disruptions. Dark blue and red points show average values over 300 pulses. Error bars are defined in Figure 10. (b) inset, shows T_{sig} on a smaller scale, together with TIE rate data from Figure 7. (c) and (d) Show images of the upper horizontal surface of divertor tile 8 at octant 8 taken (c) prior to the ILW campaign and (d) again just after JET Pulse No: 82929.

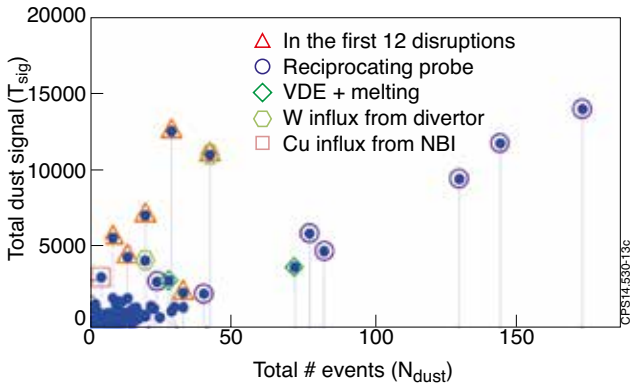

Figure 12 HRTS dust data: Total signal versus total number of events. Each data point represents a single disruption event. Additional details for extreme events are noted in the legend.

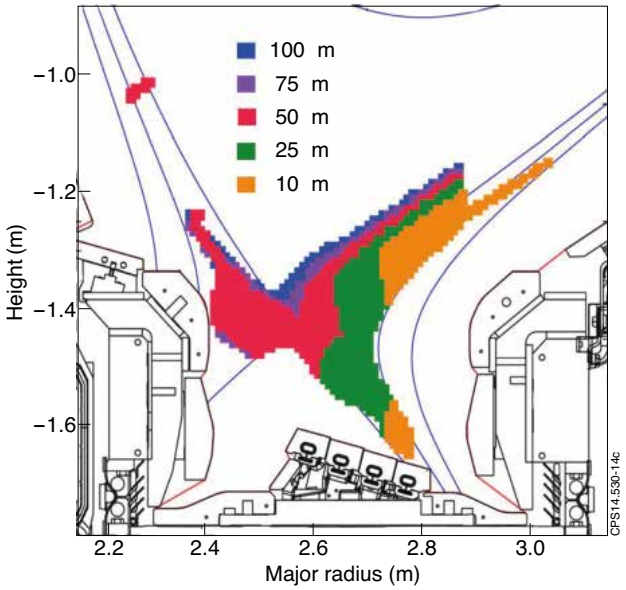

Figure 13 Polodial cross-section of JET for Pulse No: 82550 at t = 15.5s. Coloured areas indicate the average ablation position for particles of radius 100, 75, 50, 20 and 10μm, from DTOKS modelling of W particles injected from the outer strike point at